



HAL
open science

Determinant Monte Carlo algorithms for dynamical quantities in fermionic systems

Alice Moutenet, Wei Wu, Michel Ferrero

► **To cite this version:**

Alice Moutenet, Wei Wu, Michel Ferrero. Determinant Monte Carlo algorithms for dynamical quantities in fermionic systems. *Physical Review B*, 2018, 97 (8), pp.085117. 10.1103/PhysRevB.97.085117 . hal-02364078

HAL Id: hal-02364078

<https://hal.science/hal-02364078v1>

Submitted on 8 Jan 2025

HAL is a multi-disciplinary open access archive for the deposit and dissemination of scientific research documents, whether they are published or not. The documents may come from teaching and research institutions in France or abroad, or from public or private research centers.

L'archive ouverte pluridisciplinaire **HAL**, est destinée au dépôt et à la diffusion de documents scientifiques de niveau recherche, publiés ou non, émanant des établissements d'enseignement et de recherche français ou étrangers, des laboratoires publics ou privés.

Determinant Monte Carlo algorithms for dynamical quantities in fermionic systems

Alice Moutenet,^{1,2} Wei Wu,^{1,2} and Michel Ferrero^{1,2}

¹*Centre de Physique Théorique, Ecole Polytechnique, CNRS, Université Paris-Saclay, 91128 Palaiseau, France*

²*Collège de France, 11 place Marcelin Berthelot, 75005 Paris, France*

(Dated: February 12, 2018)

We introduce and compare three different Monte Carlo determinantal algorithms that allow one to compute dynamical quantities, such as the self-energy, of fermionic systems in their thermodynamic limit. We show that the most efficient approach expresses the sum of a factorial number of one-particle-irreducible diagrams as a recursive sum of determinants with exponential complexity. By comparing results for the two-dimensional Hubbard model with those obtained from state-of-the-art diagrammatic Monte Carlo, we show that we can reach higher perturbation orders and greater accuracy for the same computational effort.

I. INTRODUCTION

Perturbation expansions are at the heart of many important developments in many-body physics. They appear both in the construction of new theoretical frameworks and in the design of numerical algorithms that have greatly contributed to push further our understanding of interacting quantum systems.

Continuous-time quantum Monte Carlo algorithms¹ such as CT-INT,^{2,3} CT-AUX⁴ or CT-HYB^{5,6} are examples of such algorithms. They have been a breakthrough in finding solutions of quantum impurity problems and have opened a new realm for the development of extensions of dynamical mean-field theory.^{7–12}

One of the reasons for the success of these algorithms is that they are based on a perturbation expansion of the partition function Z . The contributions to Z can be reorganized into determinants that effectively sum a factorial number of perturbation diagrams. As a result, large perturbation orders can be computed and, for smaller clusters, the strong-coupling, low-temperature regime can be addressed. These methods are however limited by the number of sites that can be treated in the auxiliary quantum impurity cluster. For large clusters the fermionic sign problem¹³ becomes very severe as temperature is decreased or interaction increased¹⁴ and it is very difficult to extrapolate the solution of the infinite size system from a limited number of small clusters.

An alternative and complementary approach is to investigate quantum systems directly in their thermodynamic limit, as in the DiagMC^{15–19} algorithm that has also benefited from great advances. With this approach, controlled results have been obtained, e.g. for the normal phase of the unitary Fermi gas,^{20,21} the ground-state phase diagram of the Hubbard model in the weak-coupling regime away from half-filling,^{22–25} and even in parts of its phase diagram where a pseudogap has already formed.²⁶

In this method, the perturbation series is written directly for the physical quantity of interest, for example the self-energy. Contributions to the series are given by individual perturbation Feynman diagrams (one-particle irreducible ones for the self-energy) that are sampled stochastically. While the sign alternation between individual diagrams is a necessary condition for the convergence of the series, it introduces a fermionic sign problem that makes it difficult to precisely compute high-order coefficients of the series. Another difficulty of the Di-

agMC approach is that it can be challenging to resum the perturbation series and obtain converged results even if many coefficients are known with great accuracy.

In order to reduce the sign problem of the DiagMC a connected determinant algorithm (CDet) has been recently introduced in Ref. 27. The key idea of the approach is to express the sum of a factorial number of connected perturbation diagrams as a sum of determinants (a similar strategy is used in an algorithm for correlated out-of-equilibrium systems).²⁸ The physical quantity of interest is then obtained by stochastically sampling these contributions. This algorithm has been shown to scale as 3^n with the perturbation order n . It has proven to give quantitative improvements in the computation of static properties such as pressure.²⁷ However, no computation of dynamical quantities with the CDet approach has been attempted so far.

In this article, we introduce and compare three different Monte Carlo determinantal algorithms that allow to compute dynamical quantities of a fermionic system. Two of them are directly based on the CDet approach, while the third algorithm, which we will show is the most efficient, is a generalization of the CDet approach to one-particle-irreducible (1PI) diagrams. It directly samples the contributions to the self-energy with a recursive algorithm scaling as $n^2 3^n$. By comparing results for the two-dimensional Hubbard model with those obtained from DiagMC, we will show that this new approach leads to much smaller error bars for the same numerical effort. It therefore represents an important alternative to compute dynamical quantities.

The article is organized as follows. In Sec. II, we briefly summarize the CDet approach introduced in Ref. 27 as it will be one of the building blocks of our proposal. In Sec. III, we present three algorithms that allow one to derive dynamical quantities. We discuss their practical implementation as a Monte Carlo method in Sec. IV. We then compare and discuss the results of these algorithms and of the DiagMC for the two-dimensional Hubbard model in Sec. V. We finally conclude in Sec. VI.

II. CONNECTED DETERMINANT APPROACH

First, we briefly summarize the CDet approach introduced in Ref. 27 as it is one of the building blocks of our proposed

algorithms. This approach provides a general scheme to compute connected correlators. For concreteness, we consider in this article models described by a non-interacting Green's function G_0 and a local interaction vertex $Un_\uparrow n_\downarrow$. This is the case for example in the Hubbard model, in some quantum impurity problems or in the simple case of an isolated Hubbard atom (that we will later use for benchmark purposes).

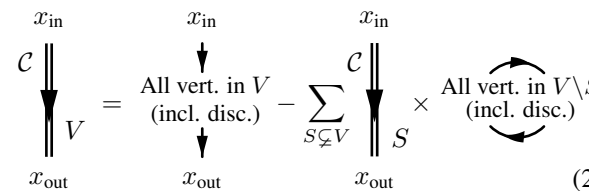
In a diagrammatic approach, a perturbation series in the interaction U is constructed. Correlation functions \mathcal{C} of two operators A and B , defined as

$$\mathcal{C}(x_{\text{out}}, x_{\text{in}}) \equiv -\langle T_\tau B(x_{\text{out}})A(x_{\text{in}}) \rangle, \quad (1)$$

where T_τ is the time-ordering operator and x denotes a vertex, are then expressed as a sum of *connected* diagrams. In real space and imaginary time, x writes (i, τ) for the Hubbard model, where i describes the lattice position and $\tau \in [0, \beta]$ the imaginary time ($\beta = 1/T$ being the inverse temperature). At a given order n in the perturbation series, a diagram contributing to $\mathcal{C}(x_{\text{out}}, x_{\text{in}})$ is characterized by the set of its internal vertices $V = \{x_1, \dots, x_n\}$ where x_l is associated with the l -th interaction vertex. The topology of such a diagram is given by two adjacency matrices describing the way the interaction vertices and the external vertices x_{in} and x_{out} are connected.

In the standard DiagMC^{15–19} technique, individual connected diagrams are stochastically sampled in a way that preserves their connectivity, with a probability given by the absolute value of their contribution to $\mathcal{C}(x_{\text{out}}, x_{\text{in}})$. Note that even if some diagrams share the same vertices, they may have alternating signs from one topology to another, which is one of the ingredients leading to a significant sign problem in this approach. The idea of the CDet algorithm is to regroup *all* diagrams sharing the same internal vertices V in a contribution $\mathcal{C}_V(x_{\text{out}}, x_{\text{in}})$, and then stochastically sample the sets V . The stochastic weight of this group of diagrams in the Monte Carlo sampling of $\mathcal{C}(x_{\text{out}}, x_{\text{in}})$ is the absolute value of their sum, which is only a function of V .

One could naturally expect that summing this factorial number of diagrams would come with a factorial cost, but it was shown²⁷ that it can actually be achieved exponentially. The sum of connected diagrams entering $\mathcal{C}_V(x_{\text{out}}, x_{\text{in}})$ is expressed as the sum of *all* diagrams (connected and disconnected ones) from which the disconnected components are recursively subtracted. This can be formalized as follows

$$\mathcal{C}_V(x_{\text{out}}, x_{\text{in}}) = \mathcal{D}_V(x_{\text{out}}, x_{\text{in}}) - \sum_{S \subsetneq V} \mathcal{C}_S(x_{\text{out}}, x_{\text{in}}) \mathcal{D}_{V \setminus S}(\emptyset),$$


$$\mathcal{C}_V(x_{\text{out}}, x_{\text{in}}) = \text{All vert. in } V \text{ (incl. disc.)} - \sum_{S \subsetneq V} \mathcal{C}_S(x_{\text{out}}, x_{\text{in}}) \times \text{All vert. in } V \setminus S \text{ (incl. disc.)} \quad (2)$$

where $\mathcal{D}_V(x_{\text{out}}, x_{\text{in}})$ denotes the sum of all diagrams (including disconnected ones) with internal vertices V , external vertices x_{in} and x_{out} . $\mathcal{D}_V(\emptyset)$ is the sum of all diagrams with vertices V and no external vertices. The cancellation of disconnected diagrams is illustrated in the second line of Eq. (2).

A key feature of this recursive sum is that \mathcal{D}_V terms can be expressed as determinants (and hence with a polynomial computational cost).²⁹

Algorithmically, the evaluation of $\mathcal{C}_V(x_{\text{out}}, x_{\text{in}})$ at order n is done in two steps. First, determinants \mathcal{D}_S are computed for all subsets S of V , with a total effort $2^n n^3$. The leading complexity however comes from the progressive computation, from low to high orders, of the \mathcal{C}_S . More precisely, if all $\mathcal{C}_{S'}$ are known for subsets S' with less than $p \leq n$ vertices, one can compute a given p -order \mathcal{C}_S using Eq. (2) with $V = S$, in 2^p operations (see r.h.s of Eq. (2)). This has to be done for all the $\binom{n}{p}$ subsets S at order p before computing contributions at the next order $p + 1$. The final result is obtained when this has been done for all $p \leq n$ and the leading complexity of the algorithm to compute $\mathcal{C}_V(x_{\text{out}}, x_{\text{in}})$ is therefore $\sum_{p=0}^n \binom{n}{p} 2^p = 3^n$.

Note that a similar cancellation of disconnected diagrams had been introduced in a quantum Monte Carlo algorithm for correlated out-of-equilibrium systems²⁸ where connected correlators are expressed as a sum of 2^n determinants thanks to Keldysh diagrammatic techniques.

The CDet approach leads to an important reduction of statistical error with respect to the DiagMC and has allowed for great progress in the computation of static properties, such as pressure in the Hubbard model.²⁷ This method, however, has not yet been used to compute dynamical quantities.

In the following, we will investigate how this can be done. We could examine, e.g. the Green's function but choose instead to focus on the self-energy Σ that is a more irreducible object where signatures of numerical noise are clearer. Other single-particle quantities can then be computed from Σ . A straightforward way to obtain Σ is to compute the Green's function G with the CDet approach and derive the self-energy through Dyson's equation. However, even if one can compute G with great accuracy, its inversion in Dyson's equation leads to an amplification of the statistical noise and, as we will show below, the resulting Σ can only be accurately obtained for low orders. It is therefore desirable to look for other techniques to compute the self-energy. This is the purpose of the following section.

III. SELF-ENERGY COMPUTATION

We introduce three different techniques to compute dynamical quantities. In order to compare their efficiencies, we focus on the self-energy Σ^σ (here σ denotes the spin) that they yield, because numerical noise is particularly visible in this quantity. First, we use Dyson's equation to obtain the self-energy from a computation of the Green's function using the CDet technique. We then present a diagrammatic method that allows us to compute the self-energy recursively from the knowledge of a different correlator \bar{F} that can still be computed using the CDet. We finally introduce an extension of the CDet algorithm that efficiently computes the sum of all *one-particle-irreducible* diagrams of a perturbation series and therefore allows us to directly stochastically sample the contributions to the self-energy. As we discuss in Sec. V, the latter allows for

a much better determination of dynamical quantities.

A. Dyson's equation

The most straightforward way to compute the self-energy Σ^σ is to first compute the Green's function G^σ using the CDet algorithm and then use Dyson's equation

$$\Sigma^\sigma = (G_0^\sigma)^{-1} - (G^\sigma)^{-1}. \quad (3)$$

We show in Sec. V that it is very difficult to obtain precise data with this method because of the inversion of G that dramatically increases the noise.

B. Equations of motion

We present a diagrammatic approach to compute the self-energy based on the computation of a different correlator with the CDet algorithm. Let us first write the self-energy as the sum of a constant Hartree term and a frequency-dependent part

$$\Sigma^\sigma(x_{\text{out}}, x_{\text{in}}) \equiv \Sigma^{H,\sigma} \delta_{x_{\text{in}}, x_{\text{out}}} + \tilde{\Sigma}^\sigma(x_{\text{out}}, x_{\text{in}}). \quad (4)$$

We recall that x is a combined index, e.g. (i, τ) for the Hubbard model, where i is the lattice site and τ the imaginary time. The Hartree term contribution is given by

$$\Sigma^{H,\sigma} \equiv U G^{\bar{\sigma}}(0^-) = \text{Diagram of a tadpole with a bubble} G^{\bar{\sigma}}(0^-) \quad (5)$$

It can be directly computed from the knowledge of the Green's function G^σ which is a connected correlator that can be obtained from Eq. (2). The self-energy Σ^σ can then be obtained recursively using the following expression

$$\Sigma^\sigma = \Sigma^{H,\sigma} + \bar{F}^\sigma - \Sigma^\sigma G^\sigma \Sigma^\sigma, \quad (6a)$$

$$\Sigma^\sigma = \text{Diagram of a tadpole} G^{\bar{\sigma}} + \text{Diagram of a bubble with two external vertices} - \text{Diagram of a bubble with two external vertices and a self-energy loop} \quad (6b)$$

where the correlation function \bar{F}^σ is defined by

$$\bar{F}^\sigma(x_{\text{out}}, x_{\text{in}}) \equiv -U^2 \langle T_\tau n_{\bar{\sigma}} c_\sigma(x_{\text{out}}) n_{\bar{\sigma}} c_\sigma^\dagger(x_{\text{in}}) \rangle. \quad (7)$$

Equation (6) can be derived from the equations of motion (EOM) of the Green's function, as detailed in Appendix A, and we will use this terminology in the following to unambiguously refer to this method. It has a simple diagrammatic interpretation, see the second line of Eq. (6), that illustrates how 1PI diagrams are isolated. Indeed, according to Eq. (4), the self-energy is the sum of contributions with a single external vertex (Hartree term $\Sigma^{H,\sigma}$) and contributions with two external vertices ($\tilde{\Sigma}^\sigma$). The former is easy to compute, and

the latter is the sum of all 1PI diagrams with two external vertices. The term \bar{F}^σ on the r.h.s of Eq. (6) represents the sum of *all connected* diagrams with the same external vertices as $\tilde{\Sigma}^\sigma$. From this, one then has to subtract all non-1PI diagrams, which can always be expressed in the form $\Sigma^\sigma G^\sigma \Sigma^\sigma$.

We now reorganize the equation above in order to be able to compute the contributions to the self-energy at a given perturbation order just from the knowledge of the contributions to \bar{F}^σ and $\Sigma^{H,\sigma}$. We first multiply Eq. (6) by G_0^σ on the right and we obtain

$$\Sigma^\sigma G_0^\sigma = \Sigma^{H,\sigma} G_0^\sigma + \bar{F}^\sigma G_0^\sigma - \Sigma^\sigma G^\sigma \Sigma^\sigma G_0^\sigma. \quad (8)$$

Reorganizing the terms,

$$\bar{F}^\sigma G_0^\sigma + \Sigma^{H,\sigma} G_0^\sigma = \Sigma^\sigma [G_0^\sigma + G^\sigma \Sigma^\sigma G_0^\sigma] = \Sigma^\sigma G^\sigma. \quad (9)$$

Substituting this expression for $\Sigma^\sigma G^\sigma$ in Eq. (6), we find

$$\Sigma^\sigma = \Sigma^{H,\sigma} + \bar{F}^\sigma - [\bar{F}^\sigma G_0^\sigma + \Sigma^{H,\sigma} G_0^\sigma] \Sigma^\sigma. \quad (10)$$

This equation allows us to recursively compute the contributions to the self-energy at all perturbation orders. Indeed, because \bar{F}^σ is at least of order 2 in U and $\Sigma^{H,\sigma}$ is at least of order 1 in U , the computation of the contribution to the self-energy at order n on the l.h.s can be obtained from the knowledge of the contributions to \bar{F} and the contributions to the self-energy at strictly lower orders $< n$ on the r.h.s. As a result, the l.h.s contributions can be computed without any inversion and there is no noise amplification as in Dyson's equation. We can therefore expect this approach to be more efficient.

The algorithm is implemented by computing the Green's function G^σ and the correlator \bar{F}^σ using the CDet algorithm. Then, Eq (10) is used to recursively compute the contributions to Σ^σ at a given order. As we use the CDet algorithm to obtain two correlators, and the self-energy is only computed in a post-processing part, the complexity of this algorithm naturally scales as 3^n .

C. Determinantal approach to sum all 1PI diagrams

We now introduce an extension of the CDet algorithm to efficiently compute the sum of all one-particle irreducible diagrams of a perturbation series. At a given perturbation order n in the interaction U , a self-energy diagram is characterized by $x_{\text{in}}, x_{\text{out}}$, its internal interaction vertices $V = \{x_1, \dots, x_{n-2}\}$, and the adjacency matrices that connect the vertices. Note that we choose $n-2$ points in the set of internal vertices V because x_{in} and x_{out} both carry an interaction vertex as well. We wish to group all diagrams that share the same internal vertices V into a contribution $\Sigma_V^\sigma(x_{\text{out}}, x_{\text{in}})$ so that

$$\begin{aligned} \Sigma^\sigma(x_{\text{out}}, x_{\text{in}}) &= \sum_V \Sigma_V^\sigma(x_{\text{out}}, x_{\text{in}}) \\ &= \sum_V \left(\Sigma_V^{H,\sigma} \delta_{x_{\text{in}}, x_{\text{out}}} + \tilde{\Sigma}_V^\sigma(x_{\text{out}}, x_{\text{in}}) \right). \end{aligned} \quad (11)$$

The contribution $\Sigma_V^\sigma(x_{\text{out}}, x_{\text{in}})$ is theoretically a sum of a factorial number of diagrams, but we will express it with the help

of a recursion, very much in the spirit of Ref. 27, that only involves connected correlators that can be computed with exponential effort using Eq. (2). The numerical effort to obtain $\tilde{\Sigma}_V^\sigma(x_{\text{out}}, x_{\text{in}})$ will then turn out to also be exponential.

The frequency-dependent part of the self-energy $\tilde{\Sigma}_V^\sigma(x_{\text{out}}, x_{\text{in}})$ can be expressed *via* the following recursive formula

$$\tilde{\Sigma}_V^\sigma(x_{\text{out}}, x_{\text{in}}) = \bar{F}_V^\sigma(x_{\text{out}}, x_{\text{in}}) - \sum_{\substack{x' \in V \\ S \subseteq V \setminus \{x'\} \\ S' = V \setminus (S \cup \{x'\})}} F_{S'}^\sigma(x_{\text{out}}, x') \tilde{\Sigma}_S^\sigma(x', x_{\text{in}}) - \sum_{\substack{S \subseteq V \\ S' = V \setminus S}} F_{S'}^\sigma(x_{\text{out}}, x_{\text{in}}) (UG_S^\sigma(0^-)), \quad (12a)$$

$$\tilde{\Sigma}_V^\sigma = \text{All vertices in } V \text{ (connected)} - \sum_{\substack{x' \in V \\ S \subseteq V \setminus \{x'\} \\ S' = V \setminus (S \cup \{x'\})}} \left\{ \tilde{\Sigma}_S^\sigma \right\} F_{S'}^\sigma - \sum_{\substack{S \subseteq V \\ S' = V \setminus S}} \left\{ G_S^\sigma \right\} F_{S'}^\sigma \quad (12b)$$

where the correlation function F^σ is given by³⁰

$$F^\sigma(x_{\text{out}}, x_{\text{in}}) = \Sigma^\sigma G^\sigma(x_{\text{out}}, x_{\text{in}}) \quad (13)$$

$$\equiv -U \langle T_\tau n_{\bar{\sigma}} c_\sigma(x_{\text{out}}) c_\sigma^\dagger(x_{\text{in}}) \rangle, \quad (14)$$

and \bar{F}^σ by Eq. (7). The starting point of the recursion is the order-2 diagram

$$x_{\text{in}} \text{---} \tilde{\Sigma}_\emptyset^\sigma \text{---} x_{\text{out}} = \text{Diagram with two external vertices } x_{\text{in}} \text{ and } x_{\text{out}} \text{ and a loop.} \quad (15)$$

The second line of Eq. (12) illustrates the cancellation of non-1PI diagrams. The self-energy contributions $\tilde{\Sigma}_V^\sigma$ that are calculated recursively are indicated as red circles, while blue diagrams correspond to the correlation function $F^\sigma = \Sigma^\sigma G^\sigma$. An explicit example of this formula at third order is shown in Appendix C. Let us note that, in this formula, the starting point of the recursion is already an order-2 diagram while it is an order-0 diagram in Eq. (2), justifying a set V with $n - 2$ vertices.

The first term $\bar{F}_V^\sigma(x_{\text{out}}, x_{\text{in}})$ on the r.h.s of Eq. (12) is the contribution to the correlation function $\bar{F}^\sigma(x_{\text{out}}, x_{\text{in}})$ for the set of internal vertices V . It is the sum of all connected diagrams that have interaction vertices at $x_{\text{in}}, x_{\text{out}}$ and all $x \in V$ as interaction vertices. In order to obtain the contributions to the self-energy $\tilde{\Sigma}_V^\sigma(x_{\text{out}}, x_{\text{in}})$, one has to subtract from this term all diagrams that are not 1PI. These ones can be expressed in the form $\Sigma^\sigma G^\sigma \Sigma^\sigma = F^\sigma \Sigma^\sigma = F^\sigma (\Sigma^{H, \sigma} + \tilde{\Sigma}^\sigma)$ and there are therefore two families of diagrams to subtract for a given set of vertices V : first all terms $F_{S'}^\sigma(x_{\text{out}}, x_{\text{in}}) \Sigma_S^{H, \sigma}$ such that $S \sqcup S' = V$, then all terms $F_{S'}^\sigma(x_{\text{out}}, x') \tilde{\Sigma}_S^\sigma(x', x_{\text{in}})$ such that $S \sqcup \{x'\} \sqcup S' = V$. In the latter family, note that $S \subsetneq V$ is a proper subset of V , so that the calculation of $\tilde{\Sigma}_V^\sigma$ involves only some $\tilde{\Sigma}_S^\sigma$ that have been previously computed in the recursion.

We have therefore derived a recursive formula for the contributions $\tilde{\Sigma}_V^\sigma(x_{\text{out}}, x_{\text{in}})$ that involves the computation of only

connected correlation functions. The recursion is completed in two steps. First, all correlators \bar{F}^σ , F^σ and G^σ have to be enumerated, the main effort coming from the F_S^σ that have to be computed for all pairs of external vertices (as a consequence of the explicit use of an intermediate vertex point x' in Eq. (12)). The computational cost for the precomputation is therefore dominated by $n^2 3^n$. Second, the recursion has to be implemented, as in the CDet, by computing the contributions $\tilde{\Sigma}_S^\sigma$ starting from low to higher orders. At a given order p , it takes an effort $p 2^p$ to get a given $\tilde{\Sigma}_S^\sigma(x', x_{\text{in}})$. This has to be done for all subsets S at order p and all x' before computing contributions at the next order $p + 1$ and requires a total effort $\binom{n}{p} p^2 2^p$. All in all the recursion will take $\sum_{p=0}^n \binom{n}{p} p^2 2^p$ with a complexity $n^2 3^n$. The leading complexity of the algorithm is therefore $n^2 3^n$.

We will show in Sec. V that despite this additional n^2 factor, this method leads to smaller error bars compared to the approaches above. It also gives more accurate results than the state-of-the-art DiagMC calculations for the same computational effort.

IV. MONTE CARLO IMPLEMENTATION

In this section, we describe how to compute the different quantities that appear in the algorithms above using a Monte Carlo (MC) method. We generically denote these quantities as \mathcal{M}^σ . The quantities that need to be computed depend on the algorithm considered. The Green's function G^σ has to be computed for all three approaches. In addition \bar{F}^σ must be computed for the equations of motion algorithm and $\tilde{\Sigma}^\sigma$ for the direct sampling of the self-energy. We write \mathcal{M}^σ as a sum over all contributions described by a set V_m with m internal vertices

$$\mathcal{M}^\sigma(x_{\text{out}}, x_{\text{in}}) = \sum_{m=0}^{\infty} \sum_{V_m} \mathcal{M}_{V_m}^\sigma(x_{\text{out}}, x_{\text{in}}). \quad (16)$$

Note that a configuration with m internal vertices contributes, in the perturbation series in U , to the coefficient of order $n = m$ for the Green's function, $n = m + 1$ for F^σ and $n = m + 2$ for $\tilde{\Sigma}^\sigma$.

In order to compute $\mathcal{M}^\sigma(x_{\text{out}}, x_{\text{in}})$, we stochastically generate Monte Carlo configurations that sample the r.h.s terms of the sum. A configuration \mathcal{C} is described by the number of internal vertices m , the spin σ and the set of all vertices

$$\mathcal{C} = \{m; \sigma; x_{\text{in}}, x_{\text{out}}; x_1, \dots, x_m\}, \quad (17)$$

and its weight in the Monte Carlo sampling is

$$w_{\mathcal{C}} = |\mathcal{M}_{V_m}^\sigma(x_{\text{out}}, x_{\text{in}})|. \quad (18)$$

We use a standard Metropolis³¹ algorithm to generate a Markov chain distributed according to $w_{\mathcal{C}}$. For concreteness, we consider the case of the Hubbard model where $x = (i, \tau)$. Starting from a given \mathcal{C} , a new configuration \mathcal{C}' is proposed by applying one of the following Monte Carlo updates:

1. Pick one of the interaction vertices in \mathcal{C} and change its position and imaginary time. One can increase the probability of the move being accepted by choosing a new position either among the neighbors of the chosen vertex or from a Gaussian distribution. The imaginary time can be chosen uniformly.
2. Flip the spin $\sigma \rightarrow \bar{\sigma}$.
3. Remove a randomly chosen internal interaction vertex from \mathcal{C} .
4. Add a new internal interaction vertex in \mathcal{C} . The new lattice site can be chosen from a Gaussian distribution around the center of gravity of the vertices in \mathcal{C} . The imaginary time can be chosen with uniform probability.

The new configuration \mathcal{C}' is accepted or rejected with the usual Metropolis ratio

$$p_{\mathcal{C} \rightarrow \mathcal{C}'}^{\text{accept}} = \min\left(1, \frac{T_{\mathcal{C}'\mathcal{C}} w_{\mathcal{C}'}}{T_{\mathcal{C}\mathcal{C}'} w_{\mathcal{C}}}\right), \quad (19)$$

where $T_{\mathcal{C}\mathcal{C}'}$ is the probability to propose \mathcal{C}' after \mathcal{C} .

This algorithm will sample the configurations according to the weights $w_{\mathcal{C}}$, however it is necessary to normalize the result. To do so, it is convenient to restrict the Monte Carlo simulation to only two consecutive orders, m and $m + 1$. A vertex can be added (resp. removed) only if the current \mathcal{C} is at order m (resp. $m + 1$). In the lowest order m the following normalization quantity is measured

$$\mathcal{N}_m = \sum_{x_{\text{in}}, x_{\text{out}}, \sigma} \sum_{V_m} |\mathcal{M}_{V_m}^\sigma(x_{\text{out}}, x_{\text{in}})|, \quad (20)$$

while at order $m + 1$, both \mathcal{N}_{m+1} and the contribution to \mathcal{M}^σ are measured. The knowledge of the expected value for \mathcal{N}_m allows us to find the normalization factor and obtain a normalized value for the contribution to \mathcal{M}^σ and \mathcal{N}_{m+1} at order $m + 1$. The latter can then be used to normalize a further simulation at orders $m + 1$ and $m + 2$, and so on. The contribution

at $m = 0$, for instance the pair-bubble diagram for the self-energy, can be computed analytically, allowing for a precise determination of \mathcal{N}_0 .

We performed several calculations for the special case of a single correlated site (especially for benchmarking purposes). In that situation, it is possible to restrict the simulation to a fixed order m and propose updates that only change the spin σ and the imaginary time of a randomly chosen interaction vertex. The normalization is obtained by computing an integral whose value is known. The simple choice

$$\mathcal{I}_m = \sum_{\sigma} \int_0^{\beta} d\tau_{\text{in}} d\tau_{\text{out}} d\tau_1 \dots d\tau_m = 2\beta^{m+2}$$

turns out to provide a good normalization.

Let us note that statistical errors in the normalization factor propagate from one order to the other. One must therefore be careful in the computation of error bars using, e.g. a binning or jackknife analysis.

V. RESULTS

In this section, we present actual computations of the self-energy according to the implementations described in Sec. III. For clarity, we respectively denote by Dyson, EOM and ΣDet the use of Dyson's equation, of the equations of motion, and of the direct calculation of the self-energy from the sum of 1PI diagrams.

We consider two models in the following. The first is a single correlated electronic level, that we will refer to as a Hubbard atom, described by the Hamiltonian

$$\mathcal{H}_{\text{atom}} = U n_{\uparrow} n_{\downarrow} + \epsilon, \quad (21)$$

where n_{σ} is the number of the spin- σ fermion, U is the onsite repulsion and ϵ the energy of the electronic level. This model has an analytical solution and allows us to both benchmark and compare the different methods introduced above. The second model is the prototypical two-dimensional Hubbard model given by

$$\mathcal{H}_{\text{Hubbard}} = -t \sum_{\langle i,j \rangle \sigma} c_{i\sigma}^{\dagger} c_{j\sigma} + U \sum_i n_{i\uparrow} n_{i\downarrow}, \quad (22)$$

where $c_{i\sigma}^{\dagger}$ creates a spin- σ electron on the site i of a square lattice, $t > 0$ is the nearest-neighbor hopping and U is the onsite interaction. This is the model that we eventually aim to solve in its thermodynamic limit (infinite lattice). In our results, $t = 1$ will be our energy unit. Note that in the computations of the Hubbard model, we use an α shift that redefines the non-interacting propagator.^{3,26,28,32}

We first benchmark our results against both analytical and standard DiagMC¹⁵⁻¹⁹ solutions and verify the theoretical complexity of our models in Appendix B. We then compare the three different methods between them, showing that ΣDet performs better both on the isolated atom and on the lattice. This method is finally shown to also improve state-of-the-art results from recent DiagMC calculations.

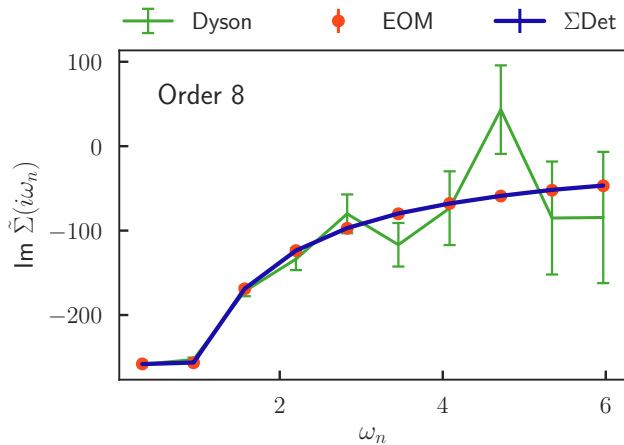


FIG. 1. Imaginary part of the Hubbard atom self-energy at order 8 in U as obtained from Dyson's equation (green), the equations of motion approach (orange) and the direct self-energy measurement (blue). We use $\beta = 10$, $U = 1$, $\epsilon = -0.2$. All simulations lasted 120 CPU hours.

A. Comparison with Dyson's equation

Until now, no dynamical quantities have been computed with the CDet algorithm and it is therefore instructive to see how the use of Dyson's equation compares to the calculation of the self-energy from the EOM and Σ Det methods.

We first consider the Hubbard atom. Figure 1 shows the contribution to the imaginary part of the Matsubara frequency self-energy $\tilde{\Sigma}^\sigma(i\omega_n)$ from perturbation order 8. The direct measurement of the self-energy and the EOM method yield results that have very small error bars (smaller than the symbol size) and that are in perfect agreement (both curves lie on top of one another). In contrast, starting from the Green's function as obtained by Eq. (2), the results for the self-energy display large statistical errors that increase with the Matsubara frequency index. The reason is simple and expected: when Dyson's equation is used to compute the self-energy, there is an amplification of the numerical noise because of the inversion of the Green's function. In practice, it becomes quickly impossible to obtain accurate data. This is problematic, because large error bars make it very difficult, e.g. to analytically continue the results to the real axis.

Figure 2 shows results for the two-dimensional Hubbard model on a 32×32 lattice (for $\beta t = 2$ the Hubbard model is in its thermodynamic limit on this lattice). At order 3, the contribution to the self-energy taken at the first Matsubara frequency $i\omega_0$ obtained from Σ Det on a chosen path in the Brillouin zone is in perfect agreement with the EOM method, and error bars for both methods are very small (smaller than symbol size, both curves being on top). The computation of Σ^σ from the Green's function is noisier. Error bars actually increase with the Matsubara frequency index when using Dyson's equation, resulting in reasonable results only for the first few frequencies even for small perturbation orders. Again, the reason for this large noise is the amplification due to the inversion of the Green's function. Also, on the lattice, a direct measurement

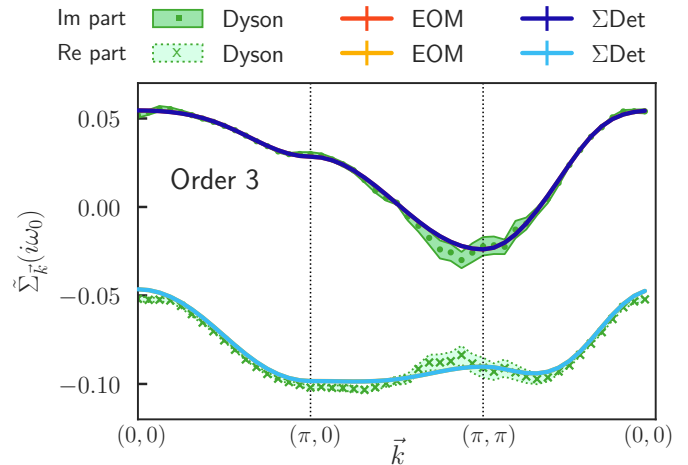


FIG. 2. Hubbard model self-energy at the first Matsubara frequency $\tilde{\Sigma}_{\vec{k}}(i\omega_0)$ along the $\vec{k} = (0,0) \rightarrow (\pi,0) \rightarrow (\pi,\pi) \rightarrow (0,0)$ path at order 3 in U , as obtained from Dyson's equation (green), the equations of motion approach (orange) and the direct self-energy measurement (blue). We use a 32×32 lattice with $\beta t = 2$, $U = 4t$, $\mu = 0$ and a uniform α shift $\alpha_\uparrow = \alpha_\downarrow = 1.53t$. All simulations lasted 120 CPU hours.

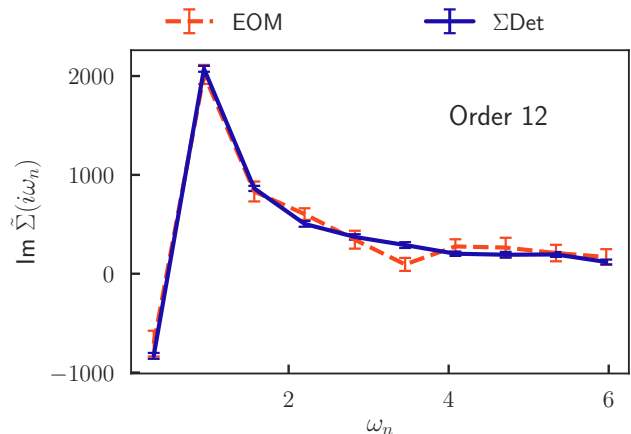


FIG. 3. Imaginary part of the Hubbard atom self-energy at order 12 in U as obtained from the equations of motion approach (orange) and the direct self-energy measurement (blue). We use $\beta = 10$, $U = 1$, $\epsilon = -0.2$. All simulations lasted 120 CPU hours.

of the self-energy has the advantage of mainly sampling fairly local diagrams. Indeed, at a temperature $T = t/2$, the self-energy very quickly vanishes for non-local components. The same is not true for the Green's function that has a slower decay; its stochastic sampling is therefore less efficient.

B. Comparison between the equations of motion and the direct sampling of the self-energy

We now compare the use of equations of motion (EOM) to the direct sampling of the self-energy expressed as a sum of IPI diagrams (Σ Det). It is not clear which method is more

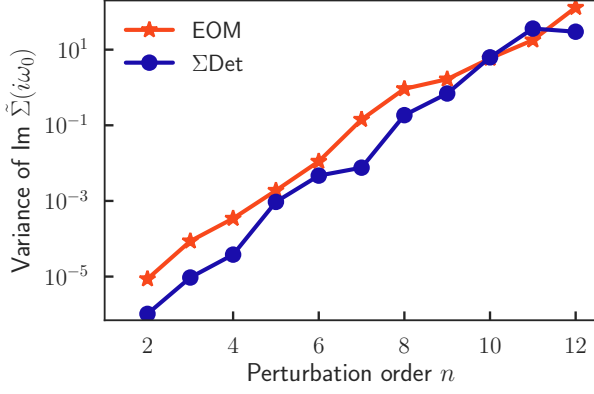


FIG. 4. Variance of the imaginary part of the Hubbard atom self-energy at the first Matsubara frequency. Orange lines with stars is the result of the equations of motion. Blue line with dots corresponds to the direct self-energy measurement. We use $\beta = 10$, $U = 1$, $\epsilon = -0.2$.

efficient, as the ΣDet allows for a precise cancellation of diagrams and directly samples the quantity of interest but scales as $n^2 3^n$, while the EOM method cancels diagrams on average but has a better scaling as 3^n .

We first consider the Hubbard atom. In Fig. 3 we show the contribution to the imaginary part of the Matsubara frequency $\tilde{\Sigma}^\sigma(i\omega_n)$ at order 12 for both methods. The equations of motion method has error bars that are seen to be about 1 order of magnitude greater than the ΣDet ones. In order to quantify the efficiency more accurately, we plot in Fig. 4 the variance at the first Matsubara frequency ω_0 as a function of the perturbation order for both methods. We see from this plot that ΣDet performs better at low perturbation order, and that both methods tend to become equivalent at higher orders.

The comparison of the resulting self-energies on the lattice Hubbard model (Fig. 5) shows an even more pronounced difference between the two approaches. At order 6, the contribution to the self-energy taken at the first Matsubara frequency (upper panel) obtained from ΣDet on a chosen path in the Brillouin zone is very well converged and the error bars for this method are very small (smaller than symbol size). The computation of Σ^σ from the equations of motion is less accurate, even if it agrees with the ΣDet within its error bars. We then look at the Matsubara frequency evolution for a given reciprocal lattice vector $\vec{k} = (\pi, \pi/2)$. The error bar for the EOM method is seen to be large for all Matsubara frequencies. To be quantitative, we plot in Fig. 6 the variance at the first Matsubara frequency ω_0 for this same value of $\vec{k} = (\pi, \pi/2)$ as function of the perturbation order. We see from this plot that ΣDet always performs better than the EOM method, by about one order of magnitude.

We believe the explanation for this behavior comes from two ingredients. First, the cancellation of non-one-particle-irreducible diagrams is done *on average* in the EOM approach, while it is exact in the ΣDet algorithm and therefore more efficient to measure the self-energy. This is particularly visible on the lattice that has more degrees of freedom. Second, the self-energy Σ^σ is more local on the lattice than the

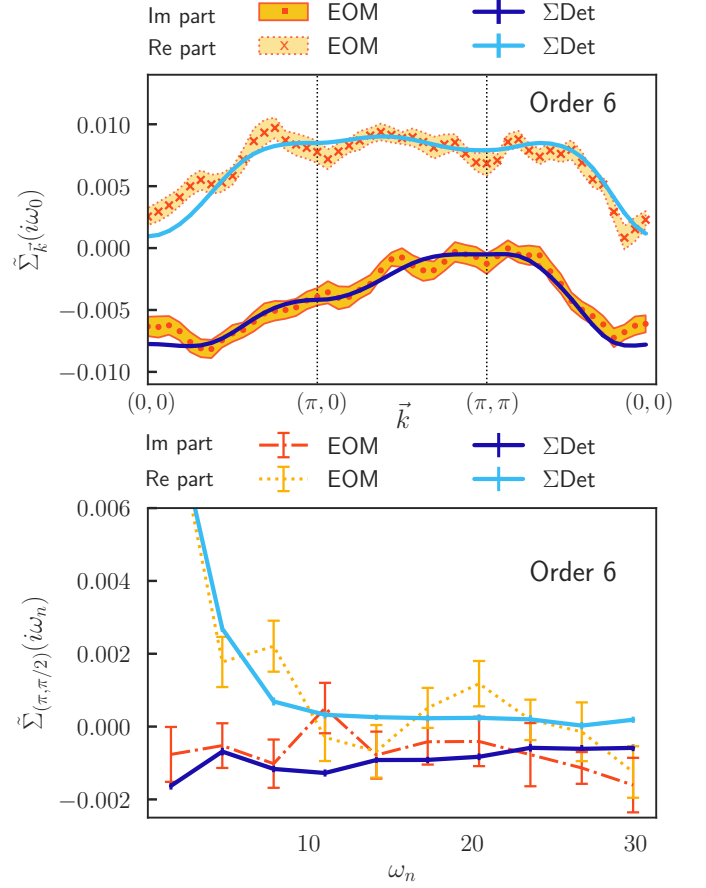


FIG. 5. Hubbard model self-energy at order 6 in U on a 32×32 lattice with $\beta t = 2$, $U = 4t$, $\mu = 0$ and with a uniform α shift $\alpha_\uparrow = \alpha_\downarrow = 1.53t$. Blue symbols are results for the direct self-energy measurement, orange symbols are results from the equations of motion approach. *Upper panel*: Self-energy at the first Matsubara frequency $\tilde{\Sigma}_{\vec{k}}(i\omega_0)$ along the $\vec{k} = (0,0) \rightarrow (\pi,0) \rightarrow (\pi,\pi) \rightarrow (0,0)$ path. *Lower panel*: Self-energy as a function of $i\omega_n$ at $\vec{k} = (\pi, \pi/2)$. All simulations lasted 120 CPU hours.

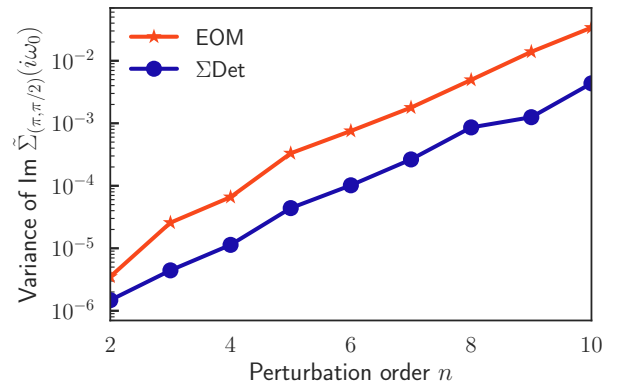


FIG. 6. Variance of the imaginary part of the Hubbard model self-energy $\text{Im } \tilde{\Sigma}_{(\pi,\pi/2)}(i\omega_0)$. Orange lines with stars is the result equations of motion. Blue line with dots corresponds to the direct self-energy measurement. We use a 32×32 lattice with $\beta t = 2$, $U = 4t$, $\mu = 0$ and with a uniform α shift $\alpha_\uparrow = \alpha_\downarrow = 1.53t$.

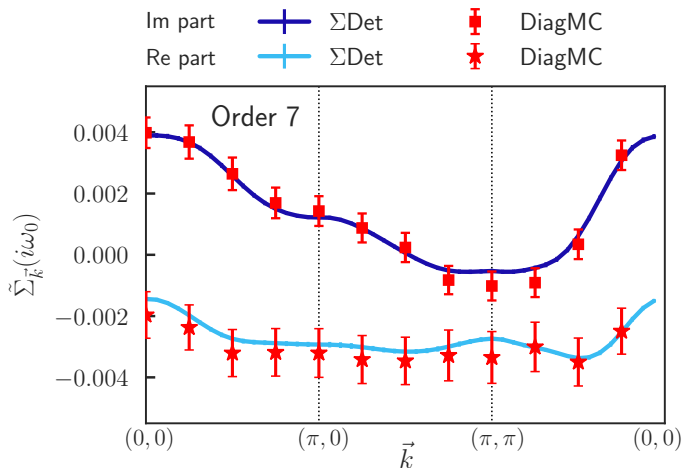


FIG. 7. Hubbard model self-energy at the first Matsubara frequency $\bar{\Sigma}_{\vec{k}}(i\omega_0)$ along the $\vec{k} = (0,0) \rightarrow (\pi,0) \rightarrow (\pi,\pi) \rightarrow (0,0)$ path at order 7 in U , as obtained from DiagMC (red) and the direct self-energy measurement (blue). We use a 32×32 lattice with $\beta t = 2$, $U = 4t$, $\mu = 0$ and a uniform α shift $\alpha_{\uparrow} = \alpha_{\downarrow} = 1.53t$. Simulations lasted 1440 CPU hours for the Σ Det and 4000 CPU hours for the DiagMC.

correlator \bar{F} . Hence the direct MC sampling of the self-energy still performs better even though its numerical complexity is greater by a factor n^2 . Let us note here that the EOM approach could be useful in the context of the real-time algorithm of Ref. 28. There the complexity of the EOM approach would be 2^n while a direct self-energy approach would scale as $n^2 3^n$. It may well be that the EOM approach is more efficient in that case.

C. Comparison between Σ Det and DiagMC algorithms

As the direct calculation of the self-energy Σ Det proves to be a very accurate method to get the self-energy, it is natural to compare it to the state-of-the-art DiagMC results on the two-dimensional Hubbard model. To this end, we compute in Fig. 7 the contribution to the first Matsubara frequency ω_0 of the self-energy at perturbation order 7 for both Σ Det and DiagMC methods. Error bars at this perturbation order, the highest currently reachable with DiagMC techniques, are much smaller with the Σ Det algorithm than with the standard DiagMC approach for simulations of the same length. This algorithm canceling directly non-1PI diagrams in the MC sampling is therefore an interesting alternative to the current diagrammatic Monte Carlo approach.

As a final illustration of the method, we compute contributions up to order 9. The resummed local self-energy is shown in Fig. 8. We observe that, with a reasonable choice for the α shift, one can completely converge the results with an uncertainty below 1%.

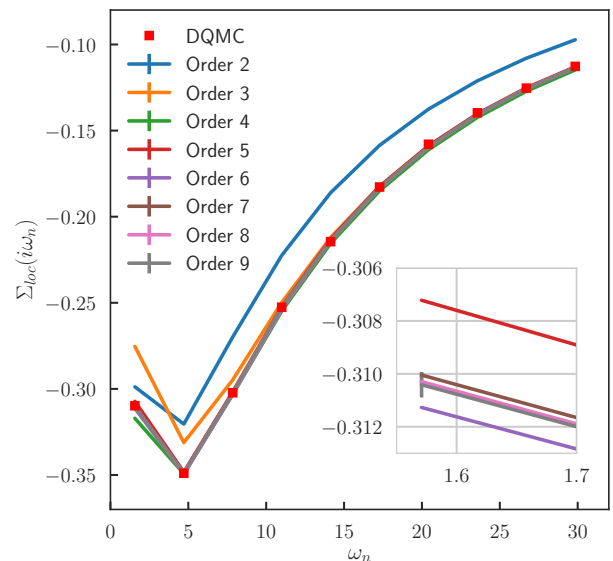


FIG. 8. Imaginary part of the local lattice self-energy $\Sigma_{\text{loc}}^{\sigma}(i\omega_n)$ as a function of Matsubara frequency, as computed using k orders, with $k = 2, \dots, 9$. The red squares are results obtained from DQMC (error bars are smaller than the symbol size). *Inset*: Zoom on the first Matsubara frequency. It is seen that the results are converged with an error bar smaller than 1%. We use a 32×32 lattice with $\beta t = 2$, $U = 4t$, $\mu = 0$ and with a uniform α shift $\alpha_{\uparrow} = \alpha_{\downarrow} = 1.53t$. The discrete time interval in DQMC is $\Delta\tau = 1/32$.

VI. CONCLUSION

We have introduced and compared three methods to compute the self-energy of fermionic systems. Two of them rely on the computation of correlators using the CDet technique, while the third one is an extension of the CDet that allows one to sum all diagrams that share the same interaction vertices and are one-particle irreducible. This allows us to design a Monte Carlo scheme that directly samples the contributions to the self-energy. This Σ Det algorithm has an exponential complexity $n^2 3^n$ where n is the perturbation order. We have shown that even if it has higher complexity, an approach that computes the self-energy directly leads to much smaller error bars with respect to the use of Dyson's equation or more sophisticated equations of motion (nevertheless, the latter could be useful in the context of real-time quantum Monte Carlo algorithms).²⁸

With the parameters that we have discussed above, $\beta = 2/t$, $U = 4t$ and $\mu = 0$ (corresponding to a total density $n = 0.66$), the direct self-energy measurement also leads to much smaller error bars than the usual DiagMC algorithm on the two-dimensional Hubbard model and sets the current state-of-the-art of these approaches. In practice, one can completely converge the results for 9 orders with an uncertainty below 1%. Note that for these parameters, other approaches, such as determinant quantum Monte Carlo (DQMC),³³ also converge (see Fig. 8). It is therefore important to more systematically compare the Σ Det approach, the DiagMC and other algorithms in different regimes of parameters in order to determine in what regions of the Hubbard model solutions can

be converged. Work is in progress along these lines (See also the recent article of Šimkovic and Kozik).³⁴

Finally, further progress is still needed to be able to reach stronger coupling regimes and lower temperatures. While the summation over all topologies certainly reduces the sign problem, the stochastic integration over imaginary times still yields large error bars at high orders. It is therefore necessary to investigate how this sign problem could be reduced.

ACKNOWLEDGMENTS

We would like to acknowledge valuable feedback from the participants of the *Diagrammatic Monte Carlo Workshop* held at the Flatiron Institute, June 2017 where this work was first presented and we are particularly grateful for discussions with A. Georges, E. Kozik, R. Rossi, F. Šimkovic and X. Waintal. We are especially indebted to O. Parcollet for suggesting improvements to our work. This work has been supported by the Simons Foundation within the Many Electron Collaboration framework (W.W.) and the European Research Council through Grant No. ERC-319286-QMAC (A.M.). Our codes were developed using the TRIQS³⁵ library. We would also like to thank the computing staff at CPHT for their help.

Appendix A: Equations of motion

Here we show that Eq. (6) can be obtained from the equations of motion of the Green's function. For concreteness, we consider the two-dimensional Hubbard model

$$\mathcal{H} = -t \sum_{\langle i,j \rangle \sigma} c_{i\sigma}^\dagger c_{j\sigma} + U \sum_i n_{i\uparrow} n_{i\downarrow} \quad (\text{A1a})$$

$$\equiv \mathcal{H}_{\text{hop}} + \mathcal{H}_{\text{int}}, \quad (\text{A1b})$$

where $c_{i\sigma}^\dagger$ creates a spin- σ electron on the site i of a square lattice, $t > 0$ is the nearest-neighbor hopping and U the on-site interaction. Note that the derivation below yields the same result for an interacting impurity coupled to a bath or for the Hubbard atom. These models are used in the article to benchmark and compare results from the different methods introduced in Sec III.

We define the imaginary-time Green's function of two operators A and B as $G_{A,B}(\tau) = -\langle T_\tau A(\tau) B(0) \rangle$. The equation of motion for G is given by

$$\partial_\tau G_{A,B}(\tau) = -\delta(\tau) \langle \{A(\tau), B(0)\} \rangle - \langle T_\tau [\mathcal{H}, A](\tau) B(0) \rangle, \quad (\text{A2})$$

which, in Matsubara frequencies, is written

$$i\omega_n G_{A,B}(i\omega_n) = -G_{[\mathcal{H},A],B}(i\omega_n) + \langle \{A, B\} \rangle. \quad (\text{A3})$$

Let us note for later use that, by writing $G_{A,B}(\tau) = -\langle T_\tau A(0) B(-\tau) \rangle$, one obtains a similar expression that involves a commutator between the Hamiltonian and B rather than A

$$i\omega_n G_{A,B}(i\omega_n) = G_{A,[\mathcal{H},B]}(i\omega_n) + \langle \{A, B\} \rangle. \quad (\text{A4})$$

The equation of motion (Eq. (A3)) for the one-particle Green's function $G_{ij}^\sigma \equiv -\langle T_\tau c_{i\sigma}(\tau) c_{j\sigma}^\dagger(0) \rangle$ is

$$i\omega_n G_{ij}^\sigma = -G_{[\mathcal{H},c_{i\sigma}],c_{j\sigma}^\dagger} + \langle \{c_{i\sigma}, c_{j\sigma}^\dagger\} \rangle. \quad (\text{A5})$$

Using the expression for the commutators

$$[\mathcal{H}_{\text{hop}}, c_{i\sigma}] = t \sum_{\langle a,b \rangle} c_{b\sigma} \delta_{ia}, \quad (\text{A6a})$$

$$[\mathcal{H}_{\text{int}}, c_{i\sigma}] = -U n_{i\bar{\sigma}} c_{i\sigma}, \quad (\text{A6b})$$

we find that

$$i\omega_n G_{ij}^\sigma = -t \sum_{\langle a,b \rangle} \delta_{ia} G_{bj}^\sigma + U G_{n_{i\bar{\sigma}} c_{i\sigma}, c_{j\sigma}^\dagger} + \delta_{ij}, \quad (\text{A7a})$$

$$\sum_{\langle a,b \rangle} (i\omega_n \delta_{ib} + t \delta_{ia}) G_{bj}^\sigma = U G_{n_{i\bar{\sigma}} c_{i\sigma}, c_{j\sigma}^\dagger} + \delta_{ij}. \quad (\text{A7b})$$

Introducing the correlator $F_{ij}^\sigma \equiv U G_{n_{i\bar{\sigma}} c_{i\sigma}, c_{j\sigma}^\dagger}$ the equation above can be rewritten in matrix form as

$$F^\sigma = (G_0^{\sigma-1} - G^{\sigma-1}) G^\sigma = \Sigma^\sigma G^\sigma. \quad (\text{A8})$$

Note that this definition of F^σ is consistent with Eq. (13). We can now apply Eq. (A4) to F_{ij}^σ

$$i\omega_n F_{ij}^\sigma = U G_{n_{i\bar{\sigma}} c_{i\sigma}, [\mathcal{H}, c_{j\sigma}^\dagger]} + U \langle \{n_{i\bar{\sigma}} c_{i\sigma}, c_{j\sigma}^\dagger\} \rangle. \quad (\text{A9})$$

Using the commutators

$$[\mathcal{H}_{\text{hop}}, c_{j\sigma}^\dagger] = -t \sum_{\langle a,b \rangle} c_{a\sigma}^\dagger \delta_{bj}, \quad (\text{A10a})$$

$$[\mathcal{H}_{\text{int}}, c_{j\sigma}^\dagger] = U n_{j\bar{\sigma}} c_{j\sigma}^\dagger, \quad (\text{A10b})$$

we find that

$$\sum_{\langle a,b \rangle} (i\omega_n \delta_{aj} + t \delta_{bj}) F_{ia}^\sigma = U^2 G_{n_{i\bar{\sigma}} c_{i\sigma}, n_{j\bar{\sigma}} c_{j\sigma}^\dagger} + \langle n_{i\bar{\sigma}} \rangle \delta_{ij}. \quad (\text{A11})$$

Introducing the correlator $\bar{F}_{ij}^\sigma \equiv U^2 G_{n_{i\bar{\sigma}} c_{i\sigma}, n_{j\bar{\sigma}} c_{j\sigma}^\dagger}$ and the Hartree term $\Sigma_{ij}^{H,\sigma} = \langle n_{i\bar{\sigma}} \rangle \delta_{ij}$ the equation above becomes

$$F^\sigma G_0^{\sigma-1} = \bar{F}^\sigma + \Sigma^{H,\sigma}. \quad (\text{A12})$$

Using Eq. (A8) for F^σ and Dyson's equation we have that

$$F^\sigma G_0^{\sigma-1} = \Sigma^\sigma G^\sigma (G^{\sigma-1} + \Sigma^\sigma) = \Sigma^\sigma + \Sigma^\sigma G^\sigma \Sigma^\sigma, \quad (\text{A13})$$

which yields the final result

$$\Sigma^\sigma = \Sigma^{H,\sigma} + \bar{F}^\sigma - \Sigma^\sigma G^\sigma \Sigma^\sigma. \quad (\text{A14})$$

This is the relation between the self-energy and the correlator \bar{F}^σ used in Eq. (6). The definitions of \bar{F}^σ and $\Sigma^{H,\sigma}$ are respectively consistent with Eqs. (7) and (5).

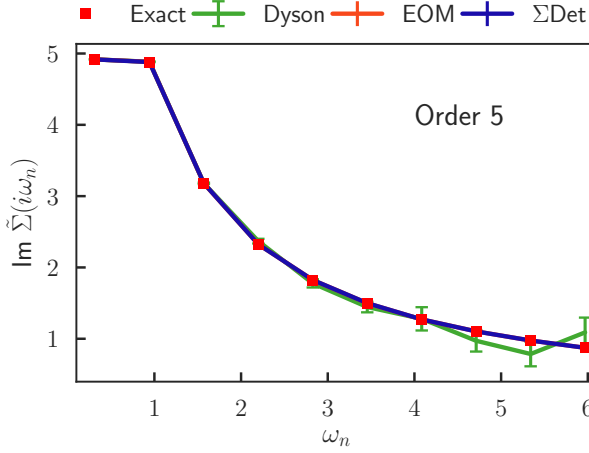


FIG. 9. Benchmark of the contribution to the Matsubara frequency self-energy $\tilde{\Sigma}(i\omega_n)$ for the Hubbard atom at order 5 in the perturbation series in U . Red squares are the analytical solution. Green lines are obtained from a calculation of the Green's function with Eq. (2). Orange line is the result of the equations of motion, and lies on top of the blue curve corresponding to the direct self-energy measurement. We use $\beta = 10$, $U = 1$, $\epsilon = -0.2$. All simulations lasted 1200 CPU hours.

Appendix B: Benchmarks

Here, we present benchmarks for the three methods introduced in the main text and we check their theoretical complexity. We first consider the simple problem of a Hubbard atom. The self-energy is given by

$$\Sigma^\sigma(i\omega_n) = \langle n_{\bar{\sigma}} \rangle U + \frac{\langle n_{\bar{\sigma}} \rangle (1 - \langle n_{\bar{\sigma}} \rangle) U^2}{i\omega_n - \epsilon - (1 - \langle n_{\bar{\sigma}} \rangle) U} \quad (\text{B1})$$

and the contributions to $\tilde{\Sigma}(i\omega_n)$ at different orders in U can be computed analytically. In Fig. 9, we show results for the contributions to $\tilde{\Sigma}(i\omega_n)$ at order 5 as obtained from the proposed algorithms. The results clearly agree with the analytical values within the error bars.

Next we consider the Hubbard model on a 32×32 square lattice. In Fig. 10 we plot the momentum-dependent self-energy $\tilde{\Sigma}_{\vec{k}}(i\omega_0)$ at its first Matsubara frequency along the $\vec{k} = (0, 0) \rightarrow (\pi, 0) \rightarrow (\pi, \pi) \rightarrow (0, 0)$ path of the Brillouin zone. Results from the three approaches are shown at order 4 and compared to results obtained using the standard DiagMC^{15–19} algorithm (This implementation of the algorithm has been benchmarked and used in earlier calculations, see e.g. Ref. 26). Results agree with the benchmark DiagMC calculation within error bars.

A measurement of the time to perform one MC step allows us to study the complexity of the algorithms. This is shown in Fig. 11, where the time for a single step is shown both for the direct measurement of the self-energy using the Σ Det and for the measurement of G using the CDet, that is then used in Dyson's equation. We know that the EOM method takes twice the CDet complexity so we consider these two methods together in this study. The expected high-order behavior in n^{23^n} for the self-energy measurement and 3^n for the

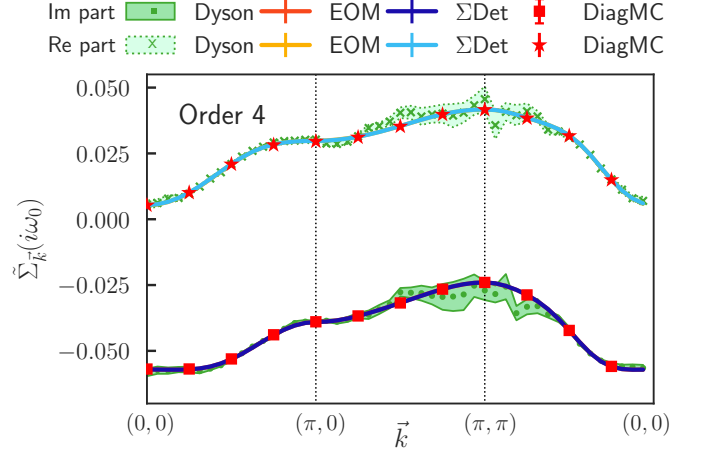


FIG. 10. Hubbard model self-energy at the first Matsubara frequency $\tilde{\Sigma}_{\vec{k}}(i\omega_0)$ along the $\vec{k} = (0, 0) \rightarrow (\pi, 0) \rightarrow (\pi, \pi) \rightarrow (0, 0)$ path at order 4 in U , as obtained from DiagMC (red), Dyson's equation (green), the equations of motion approach (orange) and the direct self-energy measurement (blue). We use a 32×32 lattice with $\beta t = 2$, $U = 4t$, $\mu = 0$ and a uniform α shift $\alpha_\uparrow = \alpha_\downarrow = 1.53t$. The DiagMC simulation lasted 400 CPU hours, while all other simulations lasted 1440 CPU hours.

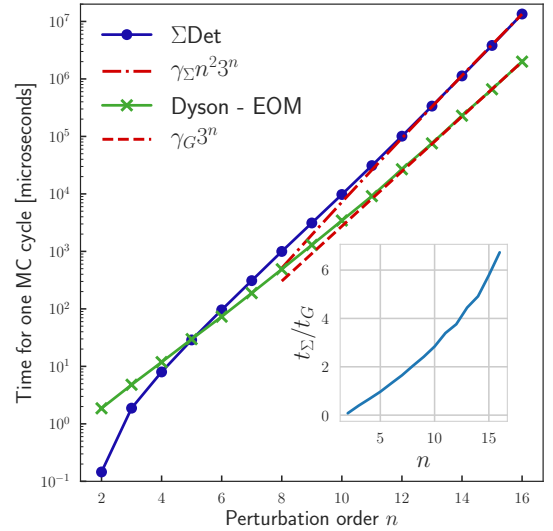


FIG. 11. Comparison of the time for one Monte Carlo cycle (in microseconds) between the direct accumulation of the self-energy (blue curve with dots) and the computation of the Green's function using CDet (green curve with dots), on a semilog scale, as a function of the perturbation order n . Each curve is fitted by its expected high- n behavior: $\gamma_\Sigma n^2 3^n$ for the Σ Det (dotted red line) and $\gamma_G 3^n$ for Dyson (dashed red line), where $\gamma_G = 0.0464$ and $\gamma_\Sigma = 0.0012$ are implementation-dependent constants. *Inset*: Ratio of the time of one MC cycle for the Σ Det (t_Σ) and for the CDet (t_G), as a function of the perturbation order n .

CDet is found. At smaller perturbation orders, the asymptotic behavior is not yet settled. At orders smaller than 5, the self-energy measurement takes less time mainly because the algorithm starts at order 2 (The recursion starts with the pair-bubble diagram, see Eq. (15) with $V = \emptyset$). On the contrary, the CDet algorithm for the Green's function starts at order 0. As a consequence, the direct measurement of the self-energy is only about a factor 3 slower than the CDet approach at order 10 (see inset of Fig. 11) which is the order that is currently accessible with reasonable error bars.

Appendix C: Cancellation of non-self-energy diagrams

Let us explicitly show the cancellation of non-self-energy diagrams in Eq. (12) for the specific case $V = \{x_1\}$ at order 3 in U . We start by considering

$$x_{\text{in}} \cdot \tilde{\Sigma}_{\emptyset}^{\sigma} \cdot x_{\text{out}} = \text{diagram} \quad (\text{C1})$$

The first term $\bar{F}_V^{\sigma}(x_{\text{out}}, x_{\text{in}})$ in Eq. (12) corresponds to all connected diagrams with two external points x_{in} and x_{out} and one internal interaction vertex x_1 :

$$\bar{F}_V^{\sigma}(x_{\text{out}}, x_{\text{in}}) = \text{diagram} + \text{diagram} + \text{diagram} + \text{diagram} + \text{diagram} + \text{diagram} \quad (\text{C2})$$

$$+ \text{diagram} + \text{diagram} + \text{diagram} + \text{diagram} + \text{diagram} + \text{diagram}$$

From this sum, we subtract the second and third terms of Eq. (12). The former gives

$$(\Sigma^{\sigma} G^{\sigma})_{\emptyset}(x_{\text{out}}, x_1) \tilde{\Sigma}_{\emptyset}^{\sigma}(x_1, x_{\text{in}}) = \text{diagram} \quad (\text{C3})$$

while the latter's contribution is the sum of

$$F_{\emptyset}^{\sigma}(x_{\text{out}}, x_{\text{in}}) \left(U G_{\{x_1\}}^{\sigma}(0^-) \right) = \text{diagram} \quad (\text{C4})$$

and of

$$F_{\{t_1\}}^{\sigma}(x_{\text{out}}, x_{\text{in}}) \left(U G_{\emptyset}^{\sigma}(0^-) \right) = \text{diagram} + \text{diagram} + \text{diagram} + \text{diagram} \quad (\text{C5})$$

We see that the remaining contributions to the self-energy that remain are only those diagrams that are one-particle irreducible.

¹ E. Gull, A. J. Millis, A. I. Lichtenstein, A. N. Rubtsov, M. Troyer, and P. Werner, *Rev. Mod. Phys.* **83**, 349 (2011).
² A. N. Rubtsov and A. I. Lichtenstein, *Journal of Experimental and Theoretical Physics Letters* **80**, 61 (2004).
³ A. N. Rubtsov, V. V. Savkin, and A. I. Lichtenstein, *Phys. Rev. B* **72**, 035122 (2005).
⁴ E. Gull, P. Werner, O. Parcollet, and M. Troyer, *EPL (Europhysics Letters)* **82**, 57003 (2008).
⁵ P. Werner, A. Comanac, L. de' Medici, M. Troyer, and A. J. Millis, *Phys. Rev. Lett.* **97**, 076405 (2006).
⁶ P. Werner and A. J. Millis, *Phys. Rev. B* **74**, 155107 (2006).
⁷ A. Georges, G. Kotliar, W. Krauth, and M. J. Rozenberg, *Rev. Mod. Phys.* **68**, 13 (1996).
⁸ G. Kotliar, S. Y. Savrasov, K. Haule, V. S. Oudovenko, O. Parcollet, and C. A. Marianetti, *Rev. Mod. Phys.* **78**, 865 (2006).
⁹ M. H. Hettler, A. N. Tahvildar-Zadeh, M. Jarrell, T. Pruschke, and H. R. Krishnamurthy, *Phys. Rev. B* **58**, R7475 (1998).
¹⁰ A. I. Lichtenstein and M. I. Katsnelson, *Phys. Rev. B* **62**, R9283 (2000).
¹¹ G. Kotliar, S. Y. Savrasov, G. Pálsson, and G. Biroli, *Phys. Rev.*

Lett. **87**, 186401 (2001).
¹² T. Maier, M. Jarrell, T. Pruschke, and M. H. Hettler, *Rev. Mod. Phys.* **77**, 1027 (2005).
¹³ M. Troyer and U.-J. Wiese, *Phys. Rev. Lett.* **94**, 170201 (2005).
¹⁴ J. P. F. LeBlanc, A. E. Antipov, F. Becca, I. W. Bulik, G. K.-L. Chan, C.-M. Chung, Y. Deng, M. Ferrero, T. M. Henderson, C. A. Jiménez-Hoyos, E. Kozik, X.-W. Liu, A. J. Millis, N. V. Prokof'ev, M. Qin, G. E. Scuseria, H. Shi, B. V. Svistunov, L. F. Tocchio, I. S. Tupitsyn, S. R. White, S. Zhang, B.-X. Zheng, Z. Zhu, and E. Gull (Simons Collaboration on the Many-Electron Problem), *Phys. Rev. X* **5**, 041041 (2015).
¹⁵ N. V. Prokof'ev and B. V. Svistunov, *Phys. Rev. Lett.* **81**, 2514 (1998).
¹⁶ N. Prokof'ev and B. Svistunov, *Phys. Rev. Lett.* **99**, 250201 (2007).
¹⁷ E. Kozik, K. V. Houcke, E. Gull, L. Pollet, N. Prokof'ev, B. Svistunov, and M. Troyer, *EPL (Europhysics Letters)* **90**, 10004 (2010).
¹⁸ K. V. Houcke, E. Kozik, N. Prokofev, and B. Svistunov, *Physics Procedia* **6**, 95 (2010), computer Simulations Studies in Con-

- densed Matter Physics XXI.
- ¹⁹ E. Bourovski, N. Prokof'ev, and B. Svistunov, *Phys. Rev. B* **70**, 193101 (2004).
- ²⁰ K. Van Houcke, F. Werner, E. Kozik, N. Prokof'ev, B. Svistunov, M. J. H. Ku, A. T. Sommer, L. W. Cheuk, A. Schirotzek, and M. W. Zwierlein, *Nat Phys* **8**, 366 (2012).
- ²¹ E. Burovski, N. Prokof'ev, B. Svistunov, and M. Troyer, *Phys. Rev. Lett.* **96**, 160402 (2006).
- ²² J. Gukelberger, L. Huang, and P. Werner, *Phys. Rev. B* **91**, 235114 (2015).
- ²³ Y. Deng, E. Kozik, N. V. Prokof'ev, and B. V. Svistunov, *EPL (Europhysics Letters)* **110**, 57001 (2015).
- ²⁴ F. Šimkovic, X.-W. Liu, Y. Deng, and E. Kozik, *Phys. Rev. B* **94**, 085106 (2016).
- ²⁵ F. Šimkovic, Y. Deng, N. V. Prokof'ev, B. V. Svistunov, I. S. Tupitsyn, and E. Kozik, *Phys. Rev. B* **96**, 081117 (2017).
- ²⁶ W. Wu, M. Ferrero, A. Georges, and E. Kozik, *Phys. Rev. B* **96**, 041105 (2017).
- ²⁷ R. Rossi, *Phys. Rev. Lett.* **119**, 045701 (2017).
- ²⁸ R. E. V. Profumo, C. Groth, L. Messio, O. Parcollet, and X. Waintal, *Phys. Rev. B* **91**, 245154 (2015).
- ²⁹ R. Rossi, N. Prokof'ev, B. Svistunov, K. V. Houcke, and F. Werner, *EPL (Europhysics Letters)* **118**, 10004 (2017).
- ³⁰ R. Bulla, A. C. Hewson, and T. Pruschke, *Journal of Physics: Condensed Matter* **10**, 8365 (1998).
- ³¹ N. Metropolis, A. W. Rosenbluth, M. N. Rosenbluth, A. H. Teller, and E. Teller, *The Journal of Chemical Physics* **21**, 1087 (1953), <http://dx.doi.org/10.1063/1.1699114>.
- ³² R. Rossi, F. Werner, N. Prokof'ev, and B. Svistunov, *Phys. Rev. B* **93**, 161102 (2016).
- ³³ R. Blankenbecler, D. J. Scalapino, and R. L. Sugar, *Phys. Rev. D* **24**, 2278 (1981).
- ³⁴ F. Šimkovic IV. and E. Kozik, *ArXiv e-prints* (2017), [arXiv:1712.10001 \[cond-mat.str-el\]](https://arxiv.org/abs/1712.10001).
- ³⁵ O. Parcollet, M. Ferrero, T. Ayrál, H. Hafermann, I. Krivenko, L. Messio, and P. Seth, *Computer Physics Communications* **196**, 398 (2015).